The Astronomical Journal, 165:147 (11pp), 2023 April https://doi.org/10.3847/1538-3881/acbafa

The Main Problem of Lunar Orbit Revisited

Bo-Sheng Li[1,2,3] and Xi-Yun Hou[1,2,3]
[1] School of Astronomy and Space Science, Nanjing University, Nanjing 210023, People's Republic of China; houxiyun@nju.edu.cn
[2] Institute of Space Environment and Astrodynamics, Nanjing University, Nanjing 210023, People's Republic of China
[3] Key Laboratory of Modern Astronomy and Astrophysics, Ministry of Education, Nanjing 210023, People's Republic of China
Received 2022 October 17; revised 2023 February 3; accepted 2023 February 3; published 2023 March 7

Abstract

A novel algorithm based on the Lindstedt–Poincaré method is proposed to construct an analytical solution of the lunar orbit. Based on the analytical solution, a numerical fitting algorithm is proposed to improve the coefficients of the analytical solution so that its accuracy can reach the level of a few kilometers within 20 yr. By fitting our solution to the long-term JPL ephemerides, we are able to recover the receding speed of the Moon from the Earth due to tidal effects. The proposed algorithm also provides a general way to treat the third-body perturbation in rectangular coordinates.

Unified Astronomy Thesaurus concepts: Lunar theory (975); Perturbation methods (1215); Orbital motion (1179)

Supporting material: machine-readable table

1. Introduction

Present lunar ephemerides are highly accurate due to great observational data, highly accurate models, and rapid development of numerical tools. For example, the orbit of the Moon given by the latest public JPL ephemerides DE440 is consistent with the recent data of Lunar Laser Ranging (LLR) ranges in the centimeter-level root-mean-square (rms) residual. The dynamical model currently used to generate the numerical ephemerides is complicated, including nonspherical gravitational interaction, tide effect, gravito-magnetic effect, rotation, etc. (Park et al. 2021), so producing the numerical ephemerides is a heavy task and requires considerable computations. On the other hand, the results are simple, usually in the form of storage files and simple routines for interpolation, though the large storage files usually increase the cost of onboard storage for space missions.

The disadvantage of the lunar numerical ephemerides is that it cannot describe the time-varying lunar orbit with explicit expressions, while these explicit expressions are sometimes necessary for further analytical analysis of orbital motions in the Earth–Moon space (Díez et al. 1990; Hou & Liu 2011; Yu et al. 2017). The simplest way is to assume a circular orbit of the Moon around the Earth, leading to the well-known circular restricted three-body problem (CRTBP). An improved model for the Earth–Moon system is the bicircular problem (BCP), which partially incorporates the Sun's gravity perturbation. In this model, the lunar orbit is still assumed as a circle, and the barycenter of the Earth+Moon is assumed to be on a circular orbit around the Sun (Simó et al. 1995). This model has been extensively used in studies of orbital motions in the Earth–Moon system (Abouelmagd et al. 2021; Jorba & Nicolás 2021; Singh et al. 2021). The problem with the BCP model is that it is incoherent. An improved model called the quasi-bicircular problem (QBCP) is thus proposed (Andreu 1998). In such a model, the analytical solution of the Sun–Earth–Moon system is constructed, with a base solution of circular orbits for the Moon around the Earth, and the Earth–Moon barycenter around the Sun. Using the QBCP model, high-order analytical solutions around libration points of the Earth–Moon system are constructed. Nowadays, people have an increasing interest in utilization of the cislunar space (He & Zhu 2021; McCarthy & Howell 2021). For example, spacecraft are moving around libration points and resonance orbits in the Earth–Moon system, and the so-called Kordylewski dust cloud around the Earth–Moon triangular libration points is confirmed (Slíz-Balogh & Horváth 2019). To qualitatively assess the Moon's influence on motions in the Earth–Moon space, it is helpful to have an analytical expression of the lunar orbit with a high accuracy while maintaining as simple as possible.

There are basically three ways of forming analytical expressions of the lunar orbit. The first way is to solve the main problem of the Moon through canonical perturbations. By using the contact transformation, Delaunay reduced the Hamiltonian of the system to high orders and computed explicit expressions with small parameters (Delaunay 1860). However, according to Deprit et al. (1971b), Delaunay made mistakes not only in most of the terms beyond order 8 but also in some terms of lower orders. By using a computer to do the symbolic computations, Deprit et al. (1971a, 1971b) successfully reduced the Hamiltonian of the main problem by the Lie transformation described in Deprit (1969), reconstructed, and corrected the analytical expressions of Delaunay's theory.

Another is the Hill–Brown theory (Brouwer & Clemence 1961, chapter 12). The motion described by its original equations is confined to a plane in Hill's lunar problem, in which the solar eccentricity is ignored and the rectangular coordinate rotates with the Sun's mean motion. The Poincaré periodic orbit indicating the conjunction of the mean motion of the Sun and the Moon is taken as the base solution, and complex coordinates for the plane are introduced to make the solution expressed in the form of an exponential series. Considering the inclination of the Moon and the full solar perturbation of the main problem, E. W. Hill calculated the motion of the Moon containing perigee precession with reasonable accuracy by heavy work of manual algebraic operation. Moreover, Brown doubled the significant digits of the coefficients by the method of differential corrections. The

analytical solutions based on the Hill–Brown theory were recalculated by following researchers with the help of a computer. An example is that by Schmidt (1980), who proposed an algorithm on computers to compute the coefficients of higher-order approximations.

Different from the above two methods, Chapront-Touze (1974) solved the main problem of the lunar orbit using an existing solution as a first approximation and then corrected it by integrating the equations of motion (EOMs). They assumed a solution of a finite Fourier series, in the form of $\sum A_k \cdot \begin{matrix}\cos\varphi_k \\ \sin\varphi_k\end{matrix}$, where φ_k are combinations of angle variables related to the motion of the Sun and the Moon and A_k are constant coefficients numerically corrected by an improved iterative method originating from Chapront & Mangeney (1969), which is based on the Lagrange's planetary equation. With the development of this theory and more perturbations considered, the Fourier form of the semi-analytical solution is generalized to the form of a Poisson series. Based on the semi-analytical solution, the well-known ELP ephemerides are generated. Until now, several versions of the ephemerides have been published, including ELP2000-82, ELP2000-85, ELP2000-82B, ELP2000-96, ELP/MPP01, and ELP/MPP02 (Chapront & Francou 2003). The maximum deviation between the latest version (ELP/MPP02) and the DE405 ephemerides is 2.4 m over a century around J2000, and the maximum deviation from DE406 ephemerides is 1.4 km over five millennia.

Usually, the main problem of the lunar orbit is solved first, and then weaker planetary perturbations are considered. According to Deprit et al. (1971a), the main problem is the model in which the Earth–Moon's barycenter is assumed to move on an invariant elliptic orbit around the Sun and the Moon's elliptic orbit around the Earth is perturbed by the Sun. In our work, we propose a new way based on the Lindstedt–Poincaré method to solve the problem. The Lindstedt–Poincaré method described in Poincaré (1899) aims to find explicit solutions usually in the form of trigonometric expansions, and it is widely used to investigate periodic or quasiperiodic orbits in the restricted three-body problem (Gómez et al. 1998; Jorba & Masdemont 1999; Sheth et al. 2021; Tan et al. 2021). The main problem of lunar orbit is solved with canonical variables in the Delaunay theory and with Cartesian coordinates in the Sun–Earth rotating frame in the Hill–Brown theory. The coordinate system used in our model can be taken as the averaged Earth–Moon rotating frame. By first constructing analytical solutions for the averaged Earth–Moon system and then constructing analytical solutions incorporating the Moon's orbit eccentricity and inclination (with respect to the ecliptic plane), we successfully obtain high-order analytical solutions of the lunar orbit in the Cartesian coordinate. The solution is expressed as series expansions of the lunar orbit eccentricity and orbit inclination. One thing to note is that our method can be extended to the more general case of an orbit perturbed by a third body or third bodies.

Based on the analytical solutions obtained, we numerically fit the solution with the accurate numerical lunar ephemerides. The fitting process is classified into two types. In the first type, we extract terms with coefficients larger than a prescribed value from the analytical solution, and then numerically refine the coefficients and the basic frequencies to obtain better fitting results. The rms accuracy of the solution after fitting can reach the level of kilometers (about 1″). Every 20 yr (a little bit longer than the Metonic cycle), we generate one group of analytic ephemerides in this way. These analytic expressions can meet the requirement of most analytical studies concerning the orbital dynamics in the Earth–Moon system. In the second type, instead of fitting the coefficients and frequencies, we fit more basic parameters of the Earth–Moon system, i.e., the semimajor axis, orbit eccentricity, orbit inclination, and three basic phase angles. In this way, we are able to verify the correctness of our theory and recover the receding speed of the Moon from the Earth due to the tidal dissipation.

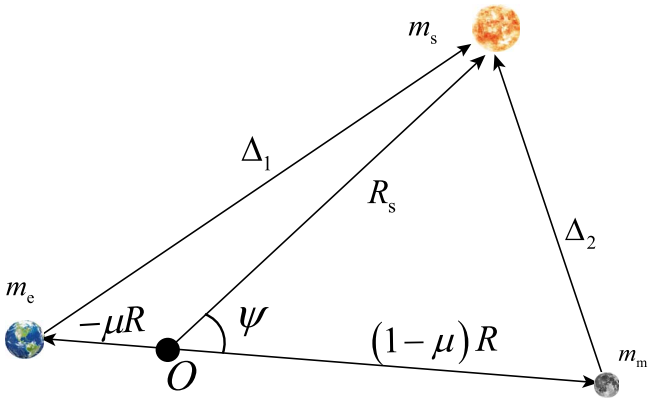

Figure 1. Relative geometry in the main problem of lunar orbit.

The paper is organized as follows. In Section 2, the dynamical model of the main problem is introduced. In Section 3, EOMs are expanded as Legendre polynomials and the reference coordinate system is introduced. In Section 4, details on the construction of high-order analytical solutions are given. To check the accuracy of the solution, a comparison between the analytical solution and numerical results of the complete EOMs is performed in Section 5. In Section 6, the first type of numerical fitting is introduced. Every 20 yr, a group of refined analytical ephemerides is generated. In Section 7, the second type of numerical fitting is introduced. The tidal effect of the Earth–Moon system is recovered. Section 8 concludes the study.

2. Model Description

It is convenient to describe the relative positions of the three mass points in Jacobi coordinates. As shown in Figure 1, the vector $\boldsymbol{R}$ points from the Earth to the Moon, $\boldsymbol{R}_s$ points from the Earth–Moon barycenter O to the Sun, and $\boldsymbol{\Delta}_1$ or $\boldsymbol{\Delta}_2$ points from the Earth or the Moon to the Sun, respectively. In addition, ψ is the angle between $\boldsymbol{R}$ and $\boldsymbol{R}_s$. Values m_e, m_m, and m_s are the masses of the three bodies. The position of barycenter between m_e and m_m depends on the mass ratio, $\mu = m_m/(m_m + m_e)$.

Plainly speaking, the main problem of lunar orbit is to solve the vector $\boldsymbol{R}$, which is disturbed by Sun's gravity, with the assumption that the orbit of the Sun with respect to the Earth–Moon barycenter is Keplerian. The difference between the real motion and the assumed Keplerian orbit of the Sun is proved to be very small in Deprit et al. (1971a) and Battin (1999).

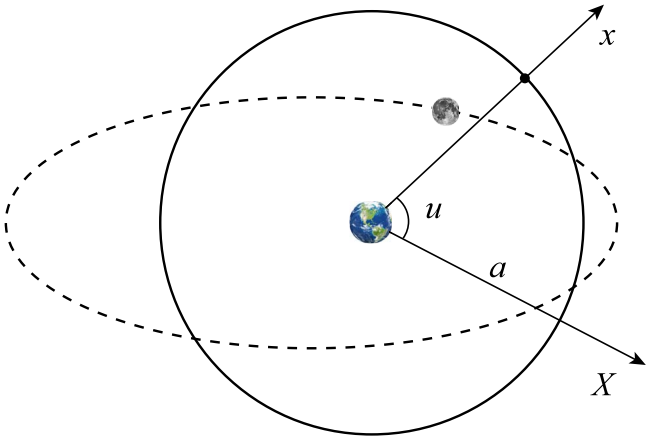

Figure 2. A perpendicular view of the reference orbit and the synodic frame rotating with the fictitious "Moon." The x-axis points to the fictitious "Moon" and the X-axis indicates the inertial frame. The angle between the X-axis and the x-axis is u.

According to Battin (1999), $\boldsymbol{R}$ and $\boldsymbol{R}_s$ follow

$$\begin{aligned}\ddot{\boldsymbol{R}} &= -G(m_e + m_m)\frac{\boldsymbol{R}}{R^3} + Gm_s\left(\frac{\boldsymbol{\Delta}_2}{\Delta_2^3} - \frac{\boldsymbol{\Delta}_1}{\Delta_1^3}\right)\\ &= \nabla_{\boldsymbol{R}}(V_e + V_s),\\ \ddot{\boldsymbol{R}}_s &= -G(m_e + m_m + m_s)\frac{\boldsymbol{R}_s}{R_s^3},\end{aligned} \tag{1}$$

in which Δ_1 or Δ_2 represents norm of the corresponding position vector, and G is the gravitational constant. The gravity is a kind of potential force, which is equal to the gradient of potential function. The potential function is divided into two parts, and their expressions are obtained by doing the inverse operation of gradient calculation. The first part $V_e = G(m_e + m_m)/R$ is the two-body potential between the Earth and the Moon, and the second part $V_s = Gm_s(\mu^{-1}\Delta_1^{-1} + (1-\mu)^{-1}\Delta_2^{-1})$ is the perturbation from the Sun.

According to Chapront-Touze (1982), the orbit inclination with respect to the ecliptic and the orbit eccentricity of the Moon are small parameters. Based on this fact, we introduce a planar reference circular orbit with a radius a, as shown by the solid circle in Figure 2. The orbit coincides with the Keplerian orbit plane of the Sun around the Earth–Moon barycenter. A fictitious "Moon" moves on this planar circular orbit with a constant angular speed $\dot{u}$. The dashed line represents an instantaneous elliptic orbit of the Moon. Actually, the reference circular orbit can be taken as the average motion of the Moon. We introduce a synodic frame rotating with the fictitious "Moon." The synodic frame has its origin at the Earth and has its axis always pointing at the fictitious "Moon." That is to say, the fictitious "Moon" stays stationary in the synodic frame. We use the lowercase letters to mark positions in the synodic frame.

In order to simplify the following derivation, we take a and $m_e + m_m$ as the units of length $[L]$ and mass $[M]$, respectively. The time unit is taken as $[T] = \sqrt{[L]^3/G[M]}$. Due to the perturbation from the Sun, the angular velocity of the fictitious averaged "Moon" no longer satisfies Kepler's third law. We denote it as

$$\dot{u} = \sqrt{G(m_e + m_m)/a^3} + \dot{\nu} = 1 + \dot{\nu}. \tag{2}$$

Because the inertial frame and the synodic frame share the same basic plane, we write the EOMs in the synodic frame by using the following transformations:

$$\boldsymbol{R} = \Gamma\boldsymbol{r},\ \dot{\boldsymbol{R}} = \dot{\Gamma}\boldsymbol{r} + \Gamma\dot{\boldsymbol{r}},\ \ddot{\boldsymbol{R}} = \ddot{\Gamma}\boldsymbol{r} + 2\dot{\Gamma}\dot{\boldsymbol{r}} + \Gamma\ddot{\boldsymbol{r}}. \tag{3}$$

Γ is the rotation matrix, which indicates a clockwise rotation of an angle u along the z-axis. Substituting Equation (3) into Equation (1), we have

$$\ddot{\boldsymbol{r}} + 2\Gamma^T\dot{\Gamma}\dot{\boldsymbol{r}} + \Gamma^T\ddot{\Gamma}\boldsymbol{r} = \nabla_{\boldsymbol{r}}(V_e + V_s), \tag{4}$$

where

$$\Gamma^T\dot{\Gamma} = \begin{pmatrix}0 & -\dot{u} & 0\\ \dot{u} & 0 & 0\\ 0 & 0 & 0\end{pmatrix},\ \Gamma^T\ddot{\Gamma} = \begin{pmatrix}-\dot{u}^2 & 0 & 0\\ 0 & -\dot{u}^2 & 0\\ 0 & 0 & 0\end{pmatrix}.$$

3. Expansion of the Potential Function and the EOMs

Denote $\boldsymbol{\rho}$ as the deviation vector from the fictitious "Moon" on the reference orbit to the instantaneous position of the real Moon. We have

$$\boldsymbol{r} = \boldsymbol{r}_0 + \boldsymbol{\rho} = (1, 0, 0)^T + (\xi, \eta, \zeta)^T, \tag{5}$$

where $\boldsymbol{r}_0$ is the position of the fictitious Moon in the synodic frame. According to the geometry in Figure 1 and Figure 2, the following relations can be obtained

$$\begin{aligned}R^{-1} &= [1 + \rho^2 - 2\rho(-\xi/\rho)]^{-1/2},\\ \Delta_i^{-1} &= (1 + x_i^2 - 2x_i\cos\psi)^{-1/2},\end{aligned} \tag{6}$$

where $i = 1$ or 2, $x_1 = -\mu r/r_s$, $x_2 = (1-\mu)r/r_s$. Taking Equation (6) as the generating function of Legendre polynomial, we have

$$\frac{1}{R} = \sum_{n=0}^{\infty}(-1)^n\rho^n P_n\left(\frac{\xi}{\rho}\right),\ \frac{1}{\Delta_i} = \sum_{n=0}^{\infty} x_i{}^n P_n(\cos\psi), \tag{7}$$

where P_n is the Legendre polynomial of order n. Substituting Equation (7) into the potential function and omitting constant terms, one can obtain the expansion of the potential function as

$$\begin{aligned}V_e &= \sum_{n=1}^{\infty} V_e^n = \sum_{n=1}^{\infty}(-1)^n\rho^n P_n\left(\frac{\xi}{\rho}\right),\\ V_s &= \sum_{n=2}^{\infty} V_s^n = \sum_{n=2}^{\infty}\frac{m_s}{a_s^3}\frac{c_n}{a_s^{n-2}}\left(\frac{a_s}{r_s}\right)^{n+1} r^n P_n(\cos\psi),\end{aligned} \tag{8}$$

where $c_n = (1-\mu)^{n-1} - (-\mu)^{n-1}$, $\cos\psi = \boldsymbol{r}\cdot\boldsymbol{r}_s/(rr_s)$, and a_s is the Sun's orbital semimajor axis. V_s can be reduced to the same form as in Battin (1999), but we keep its current form for further expansion. If the inertial X-axis, which can be arbitrarily chosen, points at the perigee of the Sun's orbit, we have the following geometric relations

$$\frac{x_s}{r_s} = \cos(f_s - u),\ \frac{y_s}{r_s} = \sin(f_s - u), \tag{9}$$

where f_s is the true anomaly of the Sun. The elliptic orbit of the Sun is expanded as a series of the eccentricity e_s and mean

anomaly M_s, in the form of

$$\begin{aligned}\frac{a_s}{r_s} &= 1 + 2\sum_{n=1}^{\infty} J_n(ne_s)\cos nM_s,\\ \cos f_s &= -e_s + \frac{2}{e_s}(1 - e_s^2)\sum_{n=1}^{\infty} J_n(ne_s)\cos nM_s,\\ \sin f_s &= 2\sqrt{1 - e_s^2}\sum_{n=1}^{\infty}\frac{1}{n}\frac{dJ_n(ne_s)}{de_s}\sin nM_s,\end{aligned} \tag{10}$$

in which $J_n(x)$ is the first kind of Bessel function. These expansions are used in the series of V_s^n. In our work, V_s is truncated at the order $n = 3$. The eccentricity is truncated at e_s^3 (in V_s^2) and e_s (in V_s^3) so that these terms with magnitude beyond 10^{-7} are neglected. The assumption of an invariant Keplerian orbit for the Earth–Moon barycenter around the Sun is no longer valid beyond this precision, so it is unnecessary to keep these higher-order terms in the truncation. Substituting Equations (5) and (8) into Equation (4), after simplification we obtain

$$\begin{aligned}\ddot{\boldsymbol{\rho}} + 2\begin{pmatrix}-\dot\eta\\ \dot\xi\\ 0\end{pmatrix} + \begin{pmatrix}-3\xi\\ 0\\ \zeta\end{pmatrix} &= \nabla_{\boldsymbol{\rho}}\left[\sum_{n=2}^{\infty}(-1)^n\rho^n P_n\left(\frac{\xi}{\rho}\right) + V_s^2 + V_s^3\right]\\ &+ 2\dot\nu\begin{pmatrix}1\\0\\0\end{pmatrix} + \dot\nu^2\begin{pmatrix}1\\0\\0\end{pmatrix} + 2\dot\nu\begin{pmatrix}\xi + \dot\eta\\ \eta - \dot\xi\\ 0\end{pmatrix} + \dot\nu^2\begin{pmatrix}\xi\\ \eta\\ 0\end{pmatrix}.\end{aligned} \tag{11}$$

It is easy to know that only the x component of the above equation has constant terms. Collecting all constant terms of the equation, we have

$$\dot\nu^2 + 2\dot\nu + \frac{m_s}{a_s^3}\left[\frac{1}{2} + \frac{3}{4}e_s^2 + \frac{9}{16a_s^2}(1 - 3\mu + 3\mu^2)\right] = 0. \tag{12}$$

There are two roots and the one with physical meaning is chosen. That is to say, the Sun's perturbation has a small influence on the mean motion of the Moon. We choose the root satisfying $\dot\nu \sim m_s/a_s^3$.

4. High-order Analytical Solution

Once we solve $\dot\nu$, the reference orbit, i.e., the fictitious Moon in the inertial frame, can be simply described as

$$X_r = a\cos((1 + \dot\nu)t), \qquad Y_r = a\sin((1 + \dot\nu)t).$$

Now the problem is to solve the deviation $\boldsymbol{\rho}$. In this section, the Lindstedt–Poincaré method is used to solve Equation (11). The coefficients of higher-order solutions can be recursively computed by substituting the low-order solutions into Equation (11) and this tedious process can be accomplished with the aid of computers. The lowest-order solution is obtained from the following linearized form of Equation (11),

$$\begin{cases}\ddot\xi - 2\dot u\dot\eta - (3 - d_1)\xi = \gamma L_\xi\\ \ddot\eta + 2\dot u\dot\xi + d_1\eta = \gamma L_\eta\\ \ddot\zeta + d_2\zeta = 0\end{cases}, \tag{13}$$

in which

$$\gamma = m_s a_s^{-3},$$

$$d_1 = \frac{9m_s c_4}{16a_s^5},\ d_2 = \frac{m_s}{a_s^3}\left(1 + \frac{3}{2}e_s^2\right) + 1.$$

The parameter γ indicates the strength of solar perturbation. L_ξ and L_η are trigonometric functions of time. Their expressions are given in Appendix A. Note that $\theta_3 = u - M_s$ and $\theta_4 = M_s$ in the expressions. Neglecting the terms L_ξ and L_η, free solutions of Equation (13) are

$$\begin{cases}\xi_{1,h} = \alpha\cos\theta_1\\ \eta_{1,h} = -\kappa\alpha\sin\theta_2,\\ \zeta_{1,h} = \beta\cos\theta_2\end{cases} \tag{14}$$

where $\theta_1 = \omega_0 t + \theta_{1,0}$, $\theta_2 = \upsilon_0 t + \theta_{2,0}$, $\kappa = (\omega_0^2 + 3 - d_1)/2\dot u\omega_0$, $\upsilon_0 = \sqrt{d_2}$, $\omega_0 = \sqrt{(4\dot u^2 + 2d_1 - 3 + \sqrt{16\dot u^4 + (16d_1 - 24)\dot u^2 + 9})/2}$. The parameters α, β are the orbit amplitudes in and out of the reference orbit plane, respectively. It is almost an immediate fact that α is proportional to Moon's orbit eccentricity e_m, and β is proportional to Moon's orbit inclination. A possible lunar orbit is defined by given values of the orbit amplitudes α, β and the initial phase angles $\theta_{1,0}$, $\theta_{2,0}$. For the Moon, in practice, there are specific values for these parameters. Note that $\omega_0 \neq \upsilon_0$ because $\dot u = 1 + \dot\nu \neq 1$. The nonhomogeneous solution caused by the terms L_ξ and L_η is

$$\begin{cases}\xi_{1,p} = \sum\xi_{00100pq}\gamma\cos(p\theta_3 + q\theta_4)\\ \eta_{1,p} = \sum\eta_{00100pq}\gamma\sin(p\theta_3 + q\theta_4)\end{cases}. \tag{15}$$

The parameter γ is already introduced in Equation (13). For the coefficients in Equation (15), the first three subscripts indicate the power of the solution and the last four subscripts indicate the linear combinations of the angles. For example, $\xi_{ijkmnpq}$ is the coefficient of $\alpha^i\beta^j\gamma^k\cos(m\theta_1 + n\theta_2 + p\theta_3 + q\theta_4)$. The order of the solution is defined as $N = i + j + k$. Substituting Equation (15) into Equation (13), it is easy to compute the coefficients. Complete solutions to the linearized system Equation (13) are

$$\begin{cases}\xi_1 = \xi_{1,h} + \xi_{1,p}\\ \eta_1 = \eta_{1,h} + \eta_{1,p}.\\ \zeta_1 = \zeta_{1,h}\end{cases} \tag{16}$$

To carry out the analysis to high orders, we utilize the properties of Legendre polynomials to rewrite the partial derivative of V_e in the same form as in Jorba & Masdemont (1999). Neglecting the derivation details, the part of

Equation (11) beyond order 2 can be rewritten as

$$\begin{cases} \ddot{\xi} - 2\dot{u}\dot{\eta} - (3 - d_1)\xi = \sum_{n\geqslant 2}(-1)^{n+1}(n+1)T_n \\ \quad +\xi\Upsilon_1^x + \eta\Upsilon_2^x + \eta\xi\Upsilon_3^x + \xi^2\Upsilon_4^x + \eta^2\Upsilon_5^x + \zeta^2\Upsilon_6^x \\ \ddot{\eta} + 2\dot{u}\dot{\xi} + d_1\eta = \eta\sum_{n\geqslant 2}(-1)^{n+1}\Phi_{n-1} \\ \quad +\xi\Upsilon_1^y + \eta\Upsilon_2^y + \eta\xi\Upsilon_3^y + \xi^2\Upsilon_4^y + \eta^2\Upsilon_5^y + \zeta^2\Upsilon_6^y \\ \ddot{\zeta} + d_2\zeta = \zeta\sum_{n\geqslant 2}(-1)^{n+1}\Phi_{n-1} \\ \quad +\zeta\Upsilon_1^z + \zeta\eta\Upsilon_2^z + \zeta\xi\Upsilon_3^z \end{cases}, \tag{17}$$

in which $T_n = \rho^n P_n\left(\frac{\xi}{\rho}\right)$, $\Phi_{n-1} = \frac{1}{\eta}\frac{\partial T_{n+1}}{\partial \eta} = \frac{1}{\zeta}\frac{\partial T_{n+1}}{\partial \zeta}$. Υ marks those terms with γ which are produced by the partial derivative of V_s, and the detailed expressions of Υ can be found in Appendix B. Although their forms seem complex, it is not difficult to calculate them on computers. In addition, following recursive relations in Jorba & Masdemont (1999) are adopted to calculate T_n and Φ_n,

$$\begin{aligned} T_n &= \frac{2n-1}{n}\xi T_{n-1} - \frac{n-1}{n}\rho^2 T_{n-2}, \\ \Phi_n &= \frac{2n+3}{n+2}\xi\Phi_{n-1} - \frac{2n+2}{n+2}T_n - \frac{n+1}{n+2}\rho^2\Phi_{n-2}, \\ T_0 &= 1,\ T_1 = \xi,\ \Phi_0 = -1,\ \Phi_1 = -3\xi. \end{aligned} \tag{18}$$

The final form of the analytical solution can be written as

$$\begin{cases} \xi = \sum \xi_{ijkmnpq}\alpha^i\beta^j\gamma^k\cos(m\theta_1 + n\theta_2 + p\theta_3 + q\theta_4) \\ \eta = \sum \eta_{ijkmnpq}\alpha^i\beta^j\gamma^k\sin(m\theta_1 + n\theta_2 + p\theta_3 + q\theta_4), \\ \zeta = \sum \zeta_{ijkmnpq}\alpha^i\beta^j\gamma^k\cos(m\theta_1 + n\theta_2 + p\theta_3 + q\theta_4) \end{cases} \tag{19}$$

where these integers i, j, k, m, n, p, q satisfy the following rules: (1) $|m| \leqslant i$, $|n| \leqslant j$, $|p| \leqslant 3n$, $|q| \leqslant 3n$; (2) m, n have the same parity as i, j, respectively; and (3) we make the sign convention that the first non-zero coefficient of $m\theta_1 + n\theta_2 + p\theta_3 + q\theta_4$ is always greater than zero.

The four angles evolve linearly with time, $\theta_i = \dot{\theta}_i t + \theta_{i,0}$. $\dot{\theta}_i$ indicate the four basic frequencies of lunar motion considered in our work. It is easy to find that $\dot{\theta}_4 = \sqrt{m_s/a_s^3}$ due to the Keplerian orbit of the Sun, and $\dot{\theta}_3 = \dot{u} - \dot{\theta}_4$ according to our definition of θ_3. The values of $\dot{\theta}_3$ and $\dot{\theta}_4$ can be immediately calculated from the Sun's parameters. $\dot{\theta}_1$, $\dot{\theta}_2$ are the power series of α, β, γ in the form

$$\dot{\theta}_1 = \sum \omega_{ijk}\alpha^i\beta^j\gamma^k,\ \dot{\theta}_2 = \sum \upsilon_{ijk}\alpha^i\beta^j\gamma^k. \tag{20}$$

In a word, the analytical solutions are trigonometric expansions with small parameters, and the four angles are linear functions of time. Only three main small parameters —the eccentricity parameter α, the inclination parameter β and the perturbation strength parameter γ—are symbolic; other small parameters such as e_s are fixed in the computation to reduce the workload of operation. The detailed algorithm of constructing the high-order analytical solution based on the Lindstedt–Poincaré method is shown in Appendix C. Theoretically, we can compute the analytical solution to arbitrary orders by the algorithm, but there may be troubles as the order increases, and we will show that in next section.

Table 1
Parameters in Numerical Simulations

Parameters	Values
a	384,388 km
Gm_e	398600.435507 $km^3\ s^{-2}$
Gm_m	4902.800118 $km^3\ s^{-2}$
Gm_s	132712440041.279419 $km^3\ s^{-2}$
α	0.055
β	0.089
$\gamma = m_s/a_s^3$	0.00557959266814
$\theta_{1,0}$, $\theta_{2,0}$	$\pi/4$
$\theta_{3,0}$	0
a_{s0}	389.183159264427
e_{s0}	0.01670236222428
M_{s0}	6.24034103140686

5. Numerical Simulations

In this section, we aim to check the accuracy of the analytic solution by comparing it with the numerical results of integrating the original EOMs (Equation (1)). Parameters of an example numerical test are shown in Table 1, in which values without a unit are dimensionless. Gm_e, Gm_m, and Gm_s are taken from Park et al. (2021). The parameters α, β take the approximate values of the Moon's mean orbital eccentricity and inclination from Simon et al. (1994). Other parameters in Table 1 take values close to real ones in the Earth–Moon system. The position and speed of the Sun are given by the JPL ephemerides DE440 at J2000 as the Sun's initial states. $\theta_{3,0} = 0$ indicates that we require the fictitious "Moon" to align with the Sun. On the other hand, the Runge–Kutta-Fehlberg (RKF78) method is used to integrate Equation (1) in the inertial frame with the initial state of the Moon given by the analytical solution. Then, the numerical results are compared with the analytical results and the deviation is plotted in Figure 3. As we can see, the deviation decreases when the order of the analytical solution increases from 4 to 6. However, the accuracy does not become better when the order of the analytical solution further increases. One should notice that the analytical solution of high orders is constructed from Equation (17), in which the potential function V_s is truncated. As a result, the accuracy of the analytical solution is restricted by this truncation. According to the numerical simulations, the analytical solution of order 6 reaches the best precision, and the maximum deviation between the numerical and the analytical solution in position is less than 4.85×10^{-5} (about $10''$) within 30 days.

The deviation rapidly increases with time, as shown in Figure 4. The reason for this increase is that the basic frequencies in the analytical solution are of limited accuracy. There are small discrepancies between the analytical frequencies and the numerical ones, and these small discrepancies cause the linear increase in the deviation. To compensate for the discrepancies, we use numerical fitting algorithms to simultaneously improve the frequencies and coefficients.

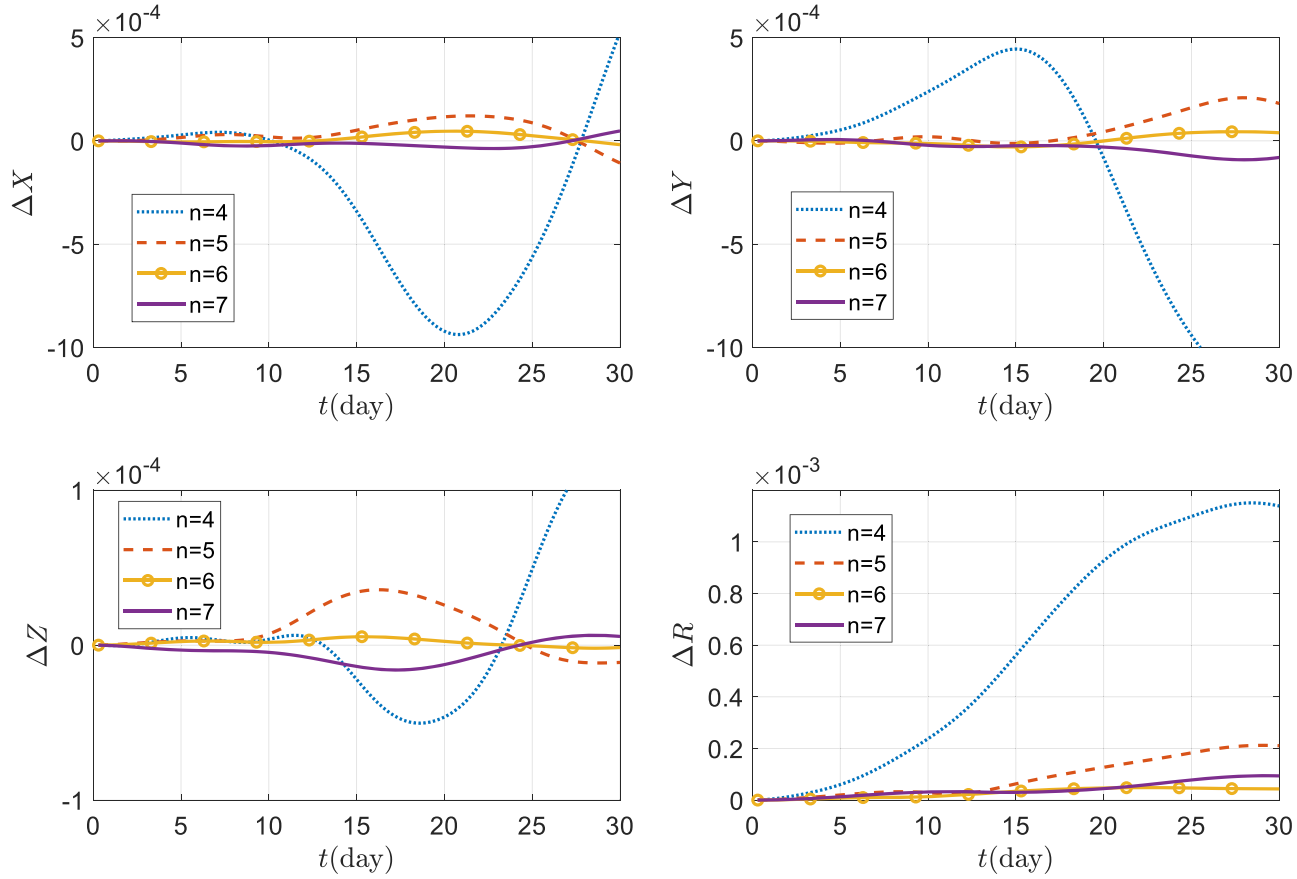

Figure 3. Position deviation between the analytical solution and the numerical one. The unit of ordinate is dimensionless. The dotted line, dashed line, solid line with circles, and solid line represent the difference between the numerical and the analytical solution of order 4, 5, 6, and 7, respectively.

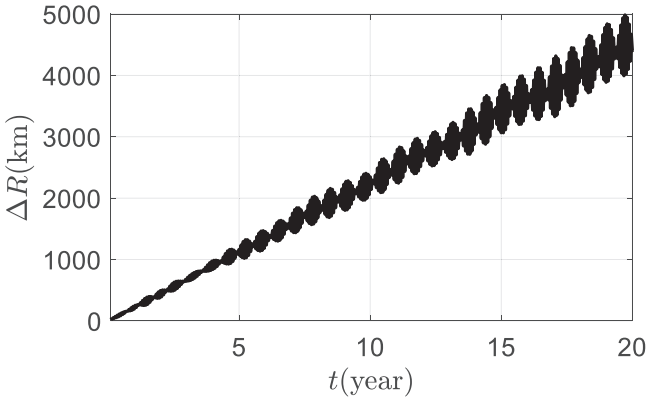

Figure 4. The secular deviation between the analytical solution of order 6 and the numerical one.

6. Numerical Fitting I

Assuming that the orbital motion of the Moon in the inertial frame is quasiperiodic, it can be written as

$$\boldsymbol{R}(t) = \begin{pmatrix} c_0^x + \sum_{i=1}^{M} (c_i^x \cos\vartheta_i + s_i^x \sin\vartheta_i) \\ c_0^y + \sum_{i=1}^{M} (c_i^y \cos\vartheta_i + s_i^y \sin\vartheta_i) \\ c_0^z + \sum_{i=1}^{M} (c_i^z \cos\vartheta_i + s_i^z \sin\vartheta_i) \end{pmatrix}, \tag{21}$$

where the integer M is the number of trigonometric terms, and ϑ_i are the linear combinations of four basic frequencies introduced in Section 4,

$$\begin{aligned} \vartheta_i &= (\boldsymbol{k}_i \cdot \boldsymbol{\omega})t, \\ \boldsymbol{\omega} &= (\dot\theta_1, \dot\theta_2, \dot\theta_3, \dot\theta_4)^T, \\ \boldsymbol{k}_i &= (m, n, p, q)^T. \end{aligned} \tag{22}$$

It is convenient to rewrite Equation (21) in the form of matrix multiplication,

$$\boldsymbol{R} = \boldsymbol{A}\boldsymbol{C}, \tag{23}$$

where $\boldsymbol{A}$ is a $3 \times (6M + 3)$ matrix,

$$\begin{aligned} \boldsymbol{A}(t) &= \begin{pmatrix} \bar{A}(t) & (0)_{1\times(2M+1)} & (0)_{1\times(2M+1)} \\ (0)_{1\times(2M+1)} & \bar{A}(t) & (0)_{1\times(2M+1)} \\ (0)_{1\times(2M+1)} & (0)_{1\times(2M+1)} & \bar{A}(t) \end{pmatrix}, \\ \bar{A}(t) &= (1, \cos\vartheta_1, \cdots, \cos\vartheta_M, \sin\vartheta_1, \cdots, \sin\vartheta_M), \end{aligned} \tag{24}$$

and $\boldsymbol{C}$ is a $(6M + 3) \times 1$ matrix embodying all the coefficients. $\boldsymbol{C} = (\boldsymbol{C}^x, \boldsymbol{C}^y, \boldsymbol{C}^z)^T$, in which

$$\begin{aligned} \boldsymbol{C}^x &= (c_0^x, c_1^x, \cdots, c_M^x, s_1^x, \cdots, s_M^x), \\ \boldsymbol{C}^y &= (c_0^y, c_1^y, \cdots, c_M^y, s_1^y, \cdots, s_M^y), \\ \boldsymbol{C}^z &= (c_0^z, c_1^z, \cdots, c_M^z, s_1^z, \cdots, s_M^z). \end{aligned} \tag{25}$$

As displayed in Figure 4, the deviation between the analytical solution and the numerical solution increases with time due to the discrepancy in the frequencies. In the following,

we will use Equation (27) to improve both the coefficients and the frequencies in order to improve the accuracy of the analytical solution. Even truncated at only order 6, there are tens of thousands of frequencies in the analytical solution, most of which have near-zero coefficients. To keep the numerical fitting process at a reasonable scale, we only pick up the terms with coefficients larger than 10^{-7} in the analytical solution (truncated at order 6) and fit them. A total of 223 frequency terms are considered in the numerical fitting.

Denote $\boldsymbol{R}_j^c$, $\boldsymbol{R}_j^o$ as the lunar positions given by the analytical solution of order 6 and observations, respectively. The subscript j represents the value taken at time t_j. In our work, the values of t_j are chosen every day within a total time interval of 100 yr. Suppose that there are N observations. The purpose of the numerical fitting is to minimize the performance index,

$$J(\boldsymbol{\omega}, \boldsymbol{C}) = \frac{1}{2N}\sum_{j=1}^{N}(\boldsymbol{R}_j^c - \boldsymbol{R}_j^o)^T(\boldsymbol{R}_j^c - \boldsymbol{R}_j^o). \tag{26}$$

N should take a value much larger than M in order to provide sufficient constraints to the coefficients of the analytic solution. In total, we have 36,525 observations in one century from the DE440 ephemerides. Every 20 yr, a numerical fitting is carried out, so the value of N is 7305 in Equation (26). The least-squares fit is used to solve the coefficients for the analytic solution. The sufficient condition for minimizing J requires

$$\partial J/\partial \boldsymbol{\omega} = 0, \quad \partial J/\partial \boldsymbol{C} = 0. \tag{27}$$

Our studies show that it is difficult to solve simultaneously both equations in Equation (27). As a result, we solve it in two steps. First, fixing the four basic frequencies as constants, we have

$$\left(\frac{\partial J}{\partial \boldsymbol{C}}\right)^T = \frac{1}{N}\sum_{j=1}^{N}\left(\frac{\partial \boldsymbol{R}_j^c}{\partial \boldsymbol{C}}\right)^T(\boldsymbol{R}_j^c - \boldsymbol{R}_j^o) = 0. \tag{28}$$

Substituting Equation (23) into Equation (28), we obtain the matrix of coefficients

$$\boldsymbol{C} = \boldsymbol{\Lambda}^{-1}\boldsymbol{B}, \tag{29}$$

where $\boldsymbol{\Lambda} = \sum_{j=1}^{N}\boldsymbol{A}_j^T\boldsymbol{A}_j$, $\boldsymbol{B} = \sum_{j=1}^{N}\boldsymbol{A}_j^T\boldsymbol{R}_j^o$.

Second, holding the coefficients matrix $\boldsymbol{C}$ obtained above constant, we numerically refine $\boldsymbol{\omega}$ from the following equations,

$$\sum_{j=1}^{N}\left(\begin{array}{l}\frac{\partial \boldsymbol{A}_j}{\partial \boldsymbol{\omega}}\boldsymbol{C} - \boldsymbol{A}_j\boldsymbol{\Lambda}^{-1}\frac{\partial \boldsymbol{\Lambda}}{\partial \boldsymbol{\omega}}\boldsymbol{C} \\ +\boldsymbol{A}_j\boldsymbol{\Lambda}^{-1}\sum_{j=1}^{N}\frac{\partial \boldsymbol{A}_j^T}{\partial \boldsymbol{\omega}}\boldsymbol{R}_j^o\end{array}\right)^T(\boldsymbol{A}_j\boldsymbol{C} - \boldsymbol{R}_j^o) = 0, \tag{30}$$

where $\frac{\partial \boldsymbol{\Lambda}}{\partial \boldsymbol{\omega}} = \sum_{j=1}^{N}\left(\frac{\partial \boldsymbol{A}_j^T}{\partial \boldsymbol{\omega}}\boldsymbol{A}_j + \boldsymbol{A}_j^T\frac{\partial \boldsymbol{A}_j}{\partial \boldsymbol{\omega}}\right)$.

Equation (30) can be solved by the Newton-Raphson algorithm. Note that we separately determine the coefficients and frequencies by taking the other as constants, so the two steps are repeated until J does not change within a prescribed accuracy.

Because the data from the JPL DE440 ephemerides is taken as observations, the inertial reference frame and the time system are in accordance with DE440. In our work, every 20 yr, a numerical fitting is carried out, and a total time interval of 100 yr, i.e., five numerical fittings are carried out. The rms of the residual, $\sqrt{2J}$ is denoted as the index of fitting precision. The best fit out of the five can reach the precision of 1.75 km (about 1″), which should be able to satisfy the needs of most analytical theories on orbital motions in the cislunar space. Table 2 shows the maximum deviation (km) and rms (km) of the five numerical fittings. One example fitting result is shown in Figure 5. The residual ΔR randomly distributes in the interval of (0 km, 6 km) during 20 yr. Table 3 lists five main trigonometric terms and corresponding coefficients. Detailed coefficients, frequencies, and dimensionless units used can be obtained from online supplementary materials for readers' reference.

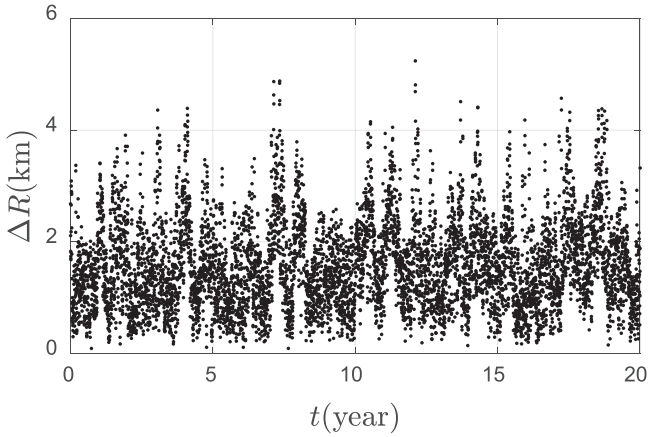

Figure 5. Residual between the best-fit analytical solution and the DE440 ephemerides. $\boldsymbol{R}_j^o$ is sampled from DE440 every day during 20 yr and the initial epoch is J2020. The rms of the residual is 1.77 km (about 1″).

Table 2
Accuracy of the Five Numerical Fittings

Epoch	Maximum Deviation			rms
	ΔX	ΔY	ΔZ	
J2000-2020	4.80	4.57	2.99	1.77
J2020-2040	4.17	4.28	3.32	1.77
J2040-2060	4.99	4.77	2.77	1.75
J2060-2080	6.78	4.97	2.78	1.76
J2080-2100	5.03	4.32	2.97	1.77

As a concluding remark, we have to admit that the accuracy of our analytical ephemerides, even after numerical fitting, is worse than that of the ELP ephemerides. The full ELP/MPP02 ephemerides involve 41,382 terms and reaches the accuracy level of meters over a century around J2000 (Chapront & Francou 2003). Our solution, although not as accurate as the ELP/MPP02 ephemerides, involves only 223 terms of frequencies. The main reasons for the worse accuracy are that we are only considering the main problem of lunar orbit instead of the complete problem, and that the solution is truncated at finite orders. Our analytical ephemerides can be used onboard spacecraft with a minimum requirement on storage while maintaining a reasonable accuracy and computation cost. Another remark is that frequencies are constant within each 20 yr interval. This means that we approximate lunar orbit as quasiperiodic motions. This assumption is very important for

Table 3
Main Terms of the Fitting Solution

m	n	p	q	c^x	s^x	c^y	s^y	c^z	s^z
0	0	1	1	0.9857559171	0.1452928858	−0.1333085139	0.9044551068	−0.0577822879	0.3920130068
0	1	0	0	0.0000046574	−0.0000150717	0.0341995759	0.0100067321	−0.0788674153	−0.0230752275
1	0	−1	−1	0.0819342349	−0.0044741496	−0.0040962251	−0.0751614620	−0.0017760288	−0.0325768889
1	0	−1	1	−0.0148433581	0.0065456055	−0.0060061503	−0.0136132546	−0.0026031595	−0.0059004851
1	0	1	1	−0.0267277651	−0.0064893042	0.0059540280	−0.0245233626	0.0025808007	−0.0106290726

Note. The complete table in machine-readable format is available. The coefficients in the table are dimensionless.
(This table is available in its entirety in machine-readable form.)

analytical theories on orbital motions in the cislunar space. We think the current ephemerides can be used in these analytical theories. Currently, we are using the analytic ephemerides to construct analytic solutions for motions that are in mean orbital resonances with the Moon.

7. Numerical Fitting II

An interesting phenomenon is that the Moon is moving away from the Earth at a speed of about 38.0 mm/year due to tidal dissipation (Folkner et al. 2014). Thus the radius of the reference orbit in our model should slowly increase with time when fitting the numerical ephemerides. The above numerical fitting avoids this problem because the coefficients and frequencies are directly fitted instead of as functions of the semimajor axis a. In this section, we use another way of numerical fitting to determine the real value of a and study its secular evolution. With the help of computers, we can easily transform the analytical solution from the reference coordinate (see Equation (19)) to the inertial frame, which is expressed in the following form

$$\begin{cases} X = \sum X_{ijkmnpq}\alpha^i\beta^j\gamma^k\cos(m\theta_1 + n\theta_2 + p\theta_3 + q\theta_4) \\ Y = \sum Y_{ijkmnpq}\alpha^i\beta^j\gamma^k\sin(m\theta_1 + n\theta_2 + p\theta_3 + q\theta_4)\,, \\ Z = \sum Z_{ijkmnpq}\alpha^i\beta^j\gamma^k\cos(m\theta_1 + n\theta_2 + p\theta_3 + q\theta_4) \end{cases} \quad (31)$$

in which these coefficients are determined by the analytical solution of order 6. Substituting the above expression into Equation (26), the performance index J is a function of variables $\boldsymbol{S}$,

$$\boldsymbol{S} = (\alpha,\ \beta,\ \gamma,\ \dot\theta_1,\ \dot\theta_2,\ \dot\theta_3,\ \dot\theta_4,\ \theta_{1,0},\ \theta_{2,0},\ \theta_{3,0},\ \theta_{4,0}). \quad (32)$$

The sufficient condition for J to take the minimum value is

$$\left(\frac{\partial J}{\partial \boldsymbol{S}}\right)^T = \frac{1}{N}\left(\frac{\partial \boldsymbol{D}}{\partial \boldsymbol{S}}\right)^T \boldsymbol{D} = 0, \quad (33)$$

where $\boldsymbol{D} = (\boldsymbol{R}_1^c - \boldsymbol{R}_1^o, \boldsymbol{R}_2^c - \boldsymbol{R}_2^o, ..., \boldsymbol{R}_j^c - \boldsymbol{R}_j^o)^T$. The Newton-Raphson algorithm is used to solve the nonlinear equations above. Denote $\boldsymbol{S}^*$, $\bar{\boldsymbol{S}}$ as the true and the approximate solution of Equation (33), respectively. Considering that $\boldsymbol{R}_i^c \to \boldsymbol{R}_i^o$ when $\bar{\boldsymbol{S}} \to \boldsymbol{S}^*$, the iterative relation is that

$$\bar{\boldsymbol{S}} - \boldsymbol{S}^* = \left(\sum_{j=1}^{N} \boldsymbol{d}_j^T \boldsymbol{d}_j\right)^{-1} \sum_{j=1}^{N} \boldsymbol{d}_j^T (\boldsymbol{R}_j^c - \boldsymbol{R}_j^o), \quad (34)$$

where $\boldsymbol{d}_j = \partial(\boldsymbol{R}_j^c - \boldsymbol{R}_j^o)/\partial \boldsymbol{S}$.

The semimajor axis a does not appear in the variable set $\boldsymbol{S}$ given by Equation (32). It is fitted by the following four steps. (1) Starting from a chosen initial epoch, we "observe" the Moon's orbit by taking values from the numerical ephemerides. Every day, one observation is taken, and the observations cover a total time length of 20 yr. (2) For an initial estimate of a, we construct the analytical solution as we did in Section 4 up to order 6 and transform the solution from the rotating frame to the inertial frame. It should be noted that the inertial frame in our model, whose reference plane is the Sun's Keplerian plane, is different from the one in the JPL ephemerides. To build a bridge between the two coordinate systems, we take the Sun's orbit relative to the Earth–Moon barycenter at the initial epoch of each fitting data in the JPL ephemerides as the inertial reference plane of our model. (3) The performance index J is computed by solving Equation (34). That is to say, from an initial estimate of the variable set $\boldsymbol{S}$, we numerically refine it to obtain the minimum value of J. (4) Changing the value of a, we repeat steps (2) and (3). In this way, we can generate the curve of J with respect to a. An example is shown in Figure 6. We believe that J reaches the minimum at the real value of a.

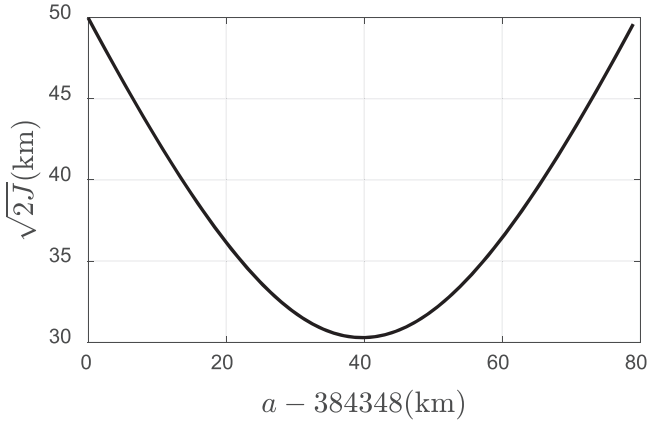

Figure 6. Curve of $\sqrt{2J}$ with respect to a. $\boldsymbol{R}_j^o$ is sampled from the DE 441 ephemerides every other day during 20 yr, and the initial epoch of this example is J2000.

In order to observe the secular drift of the Moon's orbit on a long timescale, the numerical fitting based on a 20 yr length data is performed every 1000 yr, starting from the initial epoch $JD = 1355792.5$. The data is sampled from the long-term JPL ephemerides DE 441. In total, 10 numerical fittings are carried out and the results are shown in Figure 7. As shown in the figure, the fitted semimajor axis shows a strong linear correlation with the time, and da/dt fitted with a least-square law is about 33.9 mm/yr, which is consistent with the value of 38.0 mm/yr reported in Folkner et al. (2014). The consistency further verifies our analytical solution.

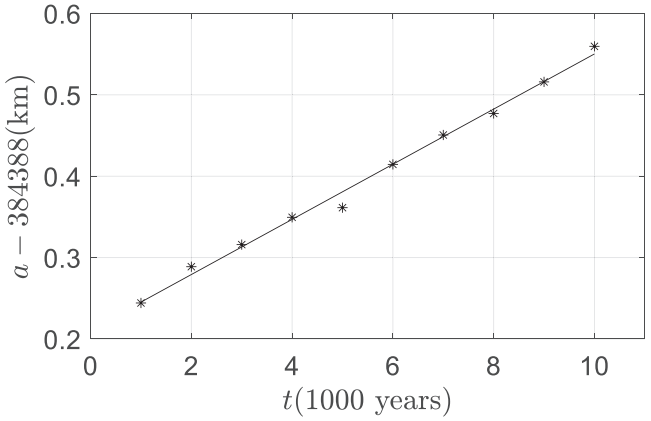

Figure 7. Semimajor axes fitted with 10 groups of data and their linear fitting based on the least-square law.

8. Conclusions

In this paper, we propose a novel algorithm based on the Lindstedt–Poincaré method to solve the main problem of lunar orbit, and successfully find its quasiperiodic analytical approximation. The analytical solution is a series of trigonometric terms as functions of three symbolic small parameters related to the Moon's eccentricity, orbital inclination, and the strength of the Sun's gravitational perturbation, and four initial phase angles. The accuracy of the analytical solution is demonstrated by a simple example. We further fit the analytical solution to the numerical ephemerides in two ways. The purpose of the first way is to improve the accuracy of the analytical solution. We successively refine the coefficients and the four basic frequencies of the analytical solution with selected terms by numerically fitting them to the JPL ephemerides DE440. Five groups of numerically fitted analytical solutions reaching the accuracy level of kilometers are obtained, covering a total time length of 100 yr. Coefficients and four basic frequencies of these five groups of analytical solutions can be found in the online materials. In our opinion, the accuracy of the fitted analytical solutions can meet the requirement of most analytical studies in the cislunar space. The purpose of the second way is to demonstrate the validity of the analytical solution. We numerically determine the radius of the reference orbit a in our model, which represents the size of the lunar orbit. The linear regression of the lunar orbit by linearly fitting 10 groups of fitted results indicates that a slightly increases on a long timescale, in accordance with the phenomenon that the Moon is moving away from the Earth due to tidal dissipation.

Because only the main problem of the lunar orbit is considered, the analytical solution truncated at a finite order can only partially approximate the Moon's real motion. The accuracy of the analytical solution of course can be further improved, by considering the complete problem, and by changing the trigonometric terms to Poisson terms as those in the ELP ephemerides. However, we decide to stop here. The main purpose of the current study is to approximate the lunar orbit as quasiperiodic motions using our new way. These quasiperiodic approximations satisfy the basic requirement for analytical studies on orbital motions in the cislunar space. They are accurate enough while maintaining a reasonable computation cost. Our studies show that within the time interval of 20 yr, the lunar orbit can be approximated as quasiperiodic motions with the rms accuracy about 1″. We intend to apply the analytical solution to analytical orbit theories (e.g., resonance orbits) in the more realistic cislunar space and some future results are on the way.

This work is supported by National Natural Science Foundation of China (No. 12233003).

Appendix A
L_ξ and L_η

$$\begin{aligned} L_\xi = {} & b_1\cos 2\theta_3 + \tfrac{51}{4}e_s^2\cos(2\theta_3-2\theta_4) \\ & + b_2\cos(2\theta_3-\theta_4) + \tfrac{845}{32}e_s^3\cos(2\theta_3-3\theta_4) \\ & + b_3\cos(2\theta_3+\theta_4) + \tfrac{1}{32}e_s^3\cos(2\theta_3+3\theta_4) \\ & + b_4\cos\theta_4 + \tfrac{9}{4}e_s^2\cos 2\theta_4 + \tfrac{53}{16}e_s^3\cos 3\theta_4 \\ & + \tfrac{c_3}{a_s}\begin{pmatrix} \tfrac{9}{8}\cos\theta_3 + \tfrac{27}{8}e_s\cos(\theta_3-\theta_4)+ \\ \tfrac{9}{8}e_s\cos(\theta_3+\theta_4) + \tfrac{15}{8}\cos 3\theta_3+ \\ \tfrac{75}{8}e_s\cos(3\theta_3-\theta_4) - \tfrac{15}{8}e_s\cos(3\theta_3+\theta_4) \end{pmatrix} \end{aligned} \tag{A1}$$

$$\begin{aligned} L_\eta = {} & -b_1\sin 2\theta_3 - \tfrac{51}{4}e_s^2\sin(2\theta_3-2\theta_4) \\ & - b_2\sin(2\theta_3-\theta_4) - \tfrac{845}{32}e_s^3\sin(2\theta_3-3\theta_4) \\ & - b_3\sin(2\theta_3+\theta_4) - \tfrac{1}{32}e_s^3\sin(2\theta_3+3\theta_4) \\ & + \tfrac{c_3}{a_s}\begin{pmatrix} -\tfrac{3}{8}\sin\theta_3 - \tfrac{9}{8}e_s\sin(\theta_3-\theta_4) \\ -\tfrac{3}{8}e_s\sin(\theta_3+\theta_4) - \tfrac{15}{8}\sin 3\theta_3 \\ -\tfrac{75}{8}e_s\sin(3\theta_3-\theta_4) + \tfrac{15}{8}e_s\sin(3\theta_3+\theta_4) \end{pmatrix}. \end{aligned} \tag{A2}$$

These coefficients in Equations (A1) and (A2) are

$$\begin{aligned} b_1 = {} & \tfrac{3}{2} - \tfrac{15}{4}e_s^2,\ b_2 = \tfrac{21}{4}e_s - \tfrac{369}{32}e_s^3, \\ b_3 = {} & -\tfrac{3}{4}e_s + \tfrac{3}{32}e_s^3,\ b_4 = \tfrac{3}{2}e_s + \tfrac{27}{16}e_s^3. \end{aligned} \tag{A3}$$

Appendix B
The Terms Produced by the Partial Derivative of V_s

$$\begin{aligned} \tfrac{\Upsilon_1^x}{\gamma} = {} & b_1\cos 2\theta_3 + \tfrac{51}{4}e_s^2\cos(2\theta_3-2\theta_4) \\ & + b_2\cos(2\theta_3-\theta_4) + b_3\cos(2\theta_3+\theta_4) \\ & + b_4\cos\theta_4 + \tfrac{9}{4}e_s^2\cos 2\theta_4 + \tfrac{1}{32}e_s^3\cos(2\theta_3+3\theta_4) \\ & + \tfrac{845}{32}e_s^3\cos(2\theta_3-3\theta_4) + \tfrac{53}{16}e_s^3\cos 3\theta_4 \\ & + \tfrac{c_3}{a_s}\begin{pmatrix} \tfrac{9}{4}\cos\theta_3 + \tfrac{27}{4}e_s\cos(\theta_3-\theta_4)+ \\ \tfrac{9}{4}e_s\cos(\theta_3+\theta_4) + \tfrac{15}{4}\cos 3\theta_3+ \\ \tfrac{75}{4}e_s\cos(3\theta_3-\theta_4) - \tfrac{15}{4}e_s\cos(3\theta_3+\theta_4) \end{pmatrix} \end{aligned} \tag{B1}$$

$$\frac{\Upsilon_2^x}{\gamma} = -\frac{51}{4}e_s^2\sin(2\theta_3 - 2\theta_4) - b_1\sin 2\theta_3 - b_2\sin(2\theta_3 - \theta_4) - b_3\sin(2\theta_3 + \theta_4) - \frac{845}{32}e_s^3\sin(2\theta_3 - 3\theta_4) - \frac{1}{32}e_s^3\sin(2\theta_3 + 3\theta_4) + \frac{c_3}{a_s}\begin{pmatrix} -\frac{15}{4}\sin 3\theta_3 - \frac{3}{4}\sin\theta_3 \\ -\frac{9}{4}e_s\sin(\theta_3 - \theta_4) - \frac{75}{4}e_s\sin(3\theta_3 - \theta_4) \\ -\frac{3}{4}e_s\sin(\theta_3 + \theta_4) + \frac{15}{4}e_s\sin(3\theta_3 + \theta_4)\end{pmatrix} \quad \text{(B2)}$$

$$\frac{\Upsilon_3^x}{\gamma} = \frac{c_3}{a_s}\begin{pmatrix} -\frac{3}{4}\sin\theta_3 - \frac{3}{4}e_s\sin(\theta_3 + \theta_4) \\ -\frac{9}{4}e_s\sin(\theta_3 - \theta_4) - \frac{75}{4}e_s\sin(3\theta_3 - \theta_4) \\ +\frac{15}{4}e_s\sin(3\theta_3 + \theta_4) - \frac{15}{4}\sin 3\theta_3\end{pmatrix} \quad \text{(B3)}$$

$$\frac{\Upsilon_4^x}{\gamma} = \frac{c_3}{a_s}\begin{pmatrix} \frac{15}{8}\cos 3\theta_3 + \frac{9}{8}\cos\theta_3 \\ +\frac{27}{8}e_s\cos(\theta_3 - \theta_4) + \frac{75}{8}e_s\cos(3\theta_3 - \theta_4) \\ +\frac{9}{8}e_s\cos(\theta_3 + \theta_4) - \frac{15}{8}e_s\cos(3\theta_3 + \theta_4)\end{pmatrix} \quad \text{(B4)}$$

$$\frac{\Upsilon_5^x}{\gamma} = \frac{c_3}{a_s}\begin{pmatrix} -\frac{15}{8}\cos 3\theta_3 + \frac{3}{8}\cos\theta_3 \\ +\frac{9}{8}e_s\cos(\theta_3 - \theta_4) - \frac{75}{8}e_s\cos(3\theta_3 - \theta_4) \\ +\frac{3}{8}e_s\cos(\theta_3 + \theta_4) + \frac{15}{8}e_s\cos(3\theta_3 + \theta_4)\end{pmatrix} \quad \text{(B5)}$$

$$\frac{\Upsilon_6^x}{\gamma} = \frac{c_3}{a_s}\begin{pmatrix} -\frac{3}{2}\cos\theta_3 - \frac{9}{2}e_s\cos(\theta_3 - \theta_4) \\ -\frac{3}{2}e_s\cos(\theta_3 + \theta_4)\end{pmatrix} \quad \text{(B6)}$$

$$\frac{\Upsilon_1^y}{\gamma} = -\frac{51}{4}e_s^2\sin(2\theta_3 - 2\theta_4) - b_1\sin 2\theta_3 - b_2\sin(2\theta_3 - \theta_4) - b_3\sin(2\theta_3 + \theta_4) - \frac{845}{32}e_s^3\sin(2\theta_3 - 3\theta_4) - \frac{1}{32}e_s^3\sin(2\theta_3 + 3\theta_4) + \frac{c_3}{a_s}\begin{pmatrix} -\frac{15}{4}\sin 3\theta_3 - \frac{3}{4}\sin\theta_3 \\ -\frac{9}{4}e_s\sin(\theta_3 - \theta_4) - \frac{75}{4}e_s\sin(3\theta_3 - \theta_4) \\ -\frac{3}{4}e_s\sin(\theta_3 + \theta_4) + \frac{15}{4}e_s\sin(3\theta_3 + \theta_4)\end{pmatrix} \quad \text{(B7)}$$

$$\frac{\Upsilon_2^y}{\gamma} = -\frac{51}{4}e_s^2\cos(2\theta_3 - 2\theta_4) - b_1\cos 2\theta_3 - b_2\cos(2\theta_3 - \theta_4) - b_3\cos(2\theta_3 + \theta_4) + b_4\cos\theta_4 + \frac{9}{4}e_s^2\cos 2\theta_4 - \frac{1}{32}e_s^3\cos(2\theta_3 + 3\theta_4) - \frac{845}{32}e_s^3\cos(2\theta_3 - 3\theta_4) + \frac{53}{16}e_s^3\cos 3\theta_4 + \frac{c_3}{a_s}\begin{pmatrix} -\frac{15}{4}\cos 3\theta_3 + \frac{3}{4}\cos\theta_3 \\ +\frac{9}{4}e_s\cos(\theta_3 - \theta_4) - \frac{75}{4}e_s\cos(3\theta_3 - \theta_4) \\ +\frac{3}{4}e_s\cos(\theta_3 + \theta_4) + \frac{15}{4}e_s\cos(3\theta_3 + \theta_4)\end{pmatrix} \quad \text{(B8)}$$

$$\frac{\Upsilon_3^y}{\gamma} = \frac{c_3}{a_s}\begin{pmatrix} -\frac{15}{4}\cos 3\theta_3 + \frac{3}{4}\cos\theta_3 \\ +\frac{9}{4}e_s\cos(\theta_3 - \theta_4) - \frac{75}{4}e_s\cos(3\theta_3 - \theta_4) \\ +\frac{3}{4}e_s\cos(\theta_3 + \theta_4) + \frac{15}{4}e_s\cos(3\theta_3 + \theta_4)\end{pmatrix} \quad \text{(B9)}$$

$$\frac{\Upsilon_4^y}{\gamma} = \frac{c_3}{a_s}\begin{pmatrix} -\frac{15}{8}\sin 3\theta_3 - \frac{3}{8}\sin\theta_3 \\ -\frac{9}{8}e_s\sin(\theta_3 - \theta_4) - \frac{75}{8}e_s\sin(3\theta_3 - \theta_4) \\ -\frac{3}{8}e_s\sin(\theta_3 + \theta_4) + \frac{15}{8}e_s\sin(3\theta_3 + \theta_4)\end{pmatrix} \quad \text{(B10)}$$

$$\frac{\Upsilon_5^y}{\gamma} = \frac{c_3}{a_s}\begin{pmatrix} \frac{15}{8}\sin 3\theta_3 - \frac{9}{8}\sin\theta_3 \\ -\frac{27}{8}e_s\sin(\theta_3 - \theta_4) + \frac{75}{8}e_s\sin(3\theta_3 - \theta_4) \\ -\frac{9}{8}e_s\sin(\theta_3 + \theta_4) - \frac{15}{8}e_s\sin(3\theta_3 + \theta_4)\end{pmatrix} \quad \text{(B11)}$$

$$\frac{\Upsilon_6^y}{\gamma} = \frac{c_3}{a_s}\begin{pmatrix} \frac{3}{2}\sin\theta_3 + \frac{9}{2}e_s\sin(\theta_3 - \theta_4) \\ +\frac{3}{2}e_s\sin(\theta_3 + \theta_4)\end{pmatrix} \quad \text{(B12)}$$

$$\frac{\Upsilon_1^z}{\gamma} = -\frac{9}{2}e_s^2\cos 2\theta_4 - \frac{53}{8}e_s^3\cos 3\theta_4 - \left(3e_s + \frac{27}{8}e_s^3\right)\cos\theta_4 + \frac{c_3}{a_s}\begin{pmatrix} -3\cos\theta_3 - 9e_s\cos(\theta_3 - \theta_4) \\ -3e_s\cos(\theta_3 + \theta_4)\end{pmatrix} \quad \text{(B13)}$$

$$\frac{\Upsilon_2^z}{\gamma} = \frac{c_3}{a_s}\begin{pmatrix} 3\sin\theta_3 + 9e_s\sin(\theta_3 - \theta_4) \\ +3e_s\sin(\theta_3 + \theta_4)\end{pmatrix} \quad \text{(B14)}$$

$$\frac{\Upsilon_3^z}{\gamma} = \frac{c_3}{a_s}\begin{pmatrix} -3\cos\theta_3 - 9e_s\cos(\theta_3 - \theta_4) \\ -3e_s\cos(\theta_3 + \theta_4)\end{pmatrix}. \quad \text{(B15)}$$

Note that the expressions of b_1, b_2, b_3, b_4 are given in Equation (A3).

Appendix C
The Algorithm of Constructing High-order Analytical Solution

Actually, the algorithm based on the Lindstedt–Poincaré method computes the coefficients in Equations (19) and (20), instead of doing a symbolic calculation of the trigonometric functions. In order to compute a certain coefficient of the solutions of order n, we need to collect the terms of the same order together and solve the following linear equations,

$$\begin{cases} -(\tau^2 + 3 - d_1)\xi_{ijkmnpq} - 2\dot{u}\tau\eta_{ijkmnpq} = \\ F^{\xi}_{ijkmnpq} + (2\omega_0 + 2\dot{u}\kappa)\omega_{i-1jk}\delta_{m1}\delta_{n0}\delta_{p0}\delta_{q0} \\ -2\dot{u}\tau\xi_{ijkmnpq} - (\tau^2 - d_1)\eta_{ijkmnpq} = \\ F^{\eta}_{ijkmnpq} + (2\omega_0\kappa + 2\dot{u})\omega_{i-1jk}\delta_{m1}\delta_{n0}\delta_{p0}\delta_{q0} \\ -\tau^2\zeta_{ijkmnpq} + d_2\zeta_{ijkmnpq} = \\ F^{\zeta}_{ijkmnpq} + 2\upsilon_0\upsilon_{ij-1k}\delta_{m0}\delta_{n1}\delta_{p0}\delta_{q0} \end{cases}, \quad \text{(C1)}$$

where $\tau = m\omega_0 + n\upsilon_0 + p\dot{\theta}_3 + q\dot{\theta}_4$, δ is Kronecker's delta,

$$\delta_{mn} = \begin{cases} 1, & m = n \\ 0, & \text{else} \end{cases},$$

and $F^{\xi}_{ijkmnpq}$, $F^{\eta}_{ijkmnpq}$, $F^{\zeta}_{ijkmnpq}$ are the coefficients of corresponding known trigonometric terms. There are two special cases when we deal with the equations above:

Case 1: $m = 1$, $n = p = q = 0$.

The first two equations of Equation (C1) are correlated due to rank deficiency of the coefficient matrix, and that the system has a solution requires a particular value for ω_{i-1jk} such that the rank of the augmented matrix equals to the rank of the

coefficient matrix. In other words, the LP method corrects the frequencies of order 0 to make the system solvable, and we have

$$\omega_{i-1jk} = \frac{(d_1 - \omega_0^2)F^{\xi}_{ijkmnpq} + 2\dot{u}\omega_0 F^{\eta}_{ijkmnpq}}{2(d_1 - \omega_0^2)(\omega_0 + \dot{u}\kappa) + 4\dot{u}\omega_0(\omega_0\kappa + \dot{u})}.$$

We normally set $F^{\xi}_{ijkmnpq} = 0$, then

$$\eta_{ijklmpq} = -\frac{F^{\xi}_{ijkmnpq} + (2\omega_0 + 2\dot{u}\kappa)\omega_{i-1jk}}{2\dot{u}\omega_0},$$

and $\zeta_{ijklmpq}$ is computed from the third equation.

Case 2: $n = 1$, $m = p = q = 0$.

The left side of the third equation of Equation (C1) equals to 0, and thus

$$\upsilon_{ij-1k} = -F^{\zeta}_{ijkmnpq} \big/ (2\upsilon_0).$$

We normally set $\zeta_{ijkmnpq} = 0$, and $\xi_{ijkmnpq}$, $\eta_{ijkmnpq}$ are computed from the first two equations.

Apart from the two cases, $\xi_{ijkmnpq}$, $\eta_{ijkmnpq}$, $\zeta_{ijkmnpq}$ can be computed by directly solving Equation (C1).

References

Abouelmagd, E. I., Mia, R., & Perdiou, A. E. 2021, ResPh, 31, 104848
Andreu, M. 1998, PhD thesis, Univ. Barcelona
Battin, R. H. 1999, An Introduction to the Mathematics and Methods of Astrodynamics (Reston, VA: AIAA), 400
Brouwer, D., & Clemence, G. M. 1961, Methods of Celestial Mechanics (1st edn.; New York: Academic Press), 335
Chapront, J., & Francou, G. 2003, A&A, 404, 735
Chapront, J., & Mangeney, L. 1969, A&A, 2, 425
Chapront-Touze, M. 1974, A&A, 36, 5
Chapront-Touze, M. 1982, CeMec, 26, 53
Delaunay, C. 1860, Mémoires de l'Académie des Sciences, Paris, 28, 882
Deprit, A. 1969, CeMec, 1, 12
Deprit, A., Henrard, J., & Rom, A. 1971a, A&A, 10, 257
Deprit, A., Henrard, J., & Rom, A. 1971b, AJ, 76, 269
Díez, C., Simó, C., & Jorba, À 1990, CeMDA, 50, 13
Folkner, W. M., Williams, J. G., Boggs, D. H., Park, R. S., & Kuchynka, P. 2014, IPNPR, 196, 42
Gómez, G., Masdemont, J., & Simó, C. 1998, JAnSc, 46, 135
He, S., & Zhu, Z. 2021, Astrodyn, 5, 61
Hou, X., & Liu, L. 2011, CeMDA, 110, 71
Jorba, A., & Masdemont, J. 1999, PhyD, 132, 189
Jorba, A., & Nicolás, B. 2021, CNSNS, 102, 105948
McCarthy, B. P., & Howell, K. C. 2021, Astrodyn, 5, 139
Park, R. S., Folkner, W. M., Williams, J. G., & Boggs, D. H. 2021, AJ, 161, 105
Poincaré, H. 1899, 1892, 1893, Les Méthodes Nouvelles de la Mécanique Céleste (Paris: Gauthier-Villars)
Schmidt, D. S. 1980, CeMec, 21, 163
Sheth, D., Thomas, V., Abouelmagd, E. I., & Srivastava, V. K. 2021, NewA, 87, 101585
Simó, C., Gómez, G., Jorba, À, & Masdemont, J. 1995, in The Bicircular Model Near the Triangular Libration Points of the RTBP, ed. A. E. Roy & B. A. Steves (Boston, MA: Springer), 343
Simon, J. L., Bretagnon, P., Chapront, J., Chapront-Touze, M., & Laskar, J. 1994, A&A, 282, 663
Singh, S. K., Anderson, B. D., Taheri, E., & Junkins, J. L. 2021, AcAau, 183, 255
Slíz-Balogh, J., & Horváth, G. 2019, MNRAS, 482, 762
Tan, P., Hou, X.-Y., & Liao, X.-H. 2021, CeMDA, 133, 31
Yu, S., Zhao, C., & Zhang, W. 2017, AdSpR, 60, 2166